Supplementary Information

Engineering the Intermediate Band States in Amorphous Ti^{3+}-doped Rutile TiO_2 for Hybrid Dye-sensitized Solar Cell Applications

Shusheng Pan[1,2⊥*], Xiaolin Liu[2⊥], Min Guo[2], Siu fung Yu[2], Haitao Huang[2], Hongtao Fan[3], Guanghai Li[1*]

[1] *Key Laboratory of Materials Physics, Anhui Key Laboratory of Nanomaterials and Nanostructures, Institute of Solid State Physics, Hefei Institutes of Physical Science, Chinese Academy of Sciences, Hefei 230031, People's Republic of China*

[2] *Department of Applied Physics, The Hong Kong Polytechnic University, Hung Hom, Kowloon, Hong Kong*

3 China National Academy of Nanotechnology and Engineering, Teda Tianjin300457, People's Republic of China

⊥ These authors contributed equally to this work

* corresponding authors: Prof. Li, ghli@issp.ac.cn, Dr. Pan, sspan@issp.ac.cn

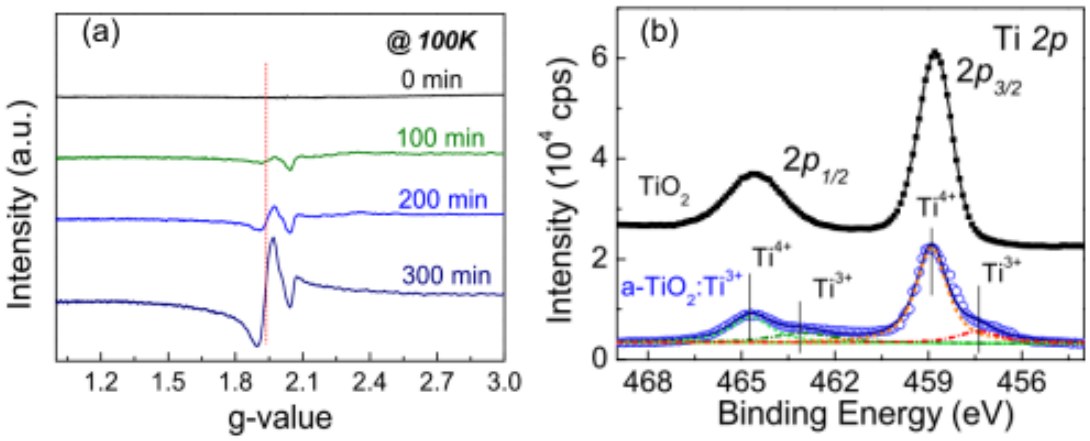

Figure S1. EPR spectra at 100 K of rutile TiO_2 nanoparticles after laser irradiation for different time intervals; (b) Ti *2p* X-ray photoelectron spectroscopy of rutile TiO2 and a-TiO_2:Ti^{3+} nanoparticles, cps: count per second.

There is a very strong EPR signal for the a-TiO_2:Ti^{3+} nanoparticles, while no signal is observed for crystalline TiO_2 nanoparticles. The intensity of the EPR signal increases with increasing laser irradiation time, indicating the increment of the Ti^{3+} concentration. The *g*-factor can be assigned to originate from the surface and subsurface paramagnetic Ti^{3+} centers, as has been previously investigated in Ti^{3+}-doped TiO_2 grown by UV light irradiation.[1,2]

For the rutile TiO_2, the binding energy peaks at 458.9 and 464.7 eV are assigned to the $2p_{3/2}$ and $2p_{1/2}$ core levels of Ti^{4+}. The fitting of the Ti $2p_{1/2}$ peak reveals the presence of two peak energies at 463.1 and 464.7 eV. The Ti $2p_{3/2}$ peak can also be resolved into two Gaussian peaks with peak energy at 457.4 and 458.9 eV. The $2p_{3/2}$ binding energy of 457.4 and 458.9 eV can be attributed to the Ti^{3+} and Ti^{4+}, respectively. The $2p_{1/2}$ core level of 463.1 and 464.7 eV are related to the Ti^{3+} and Ti^{4+}, respectively. The fitted results were shown in Table S2. These peaks are well consistent with the recently reported binding energy value of TiO_2 nanostructures containing Ti^{3+}. [3-5]

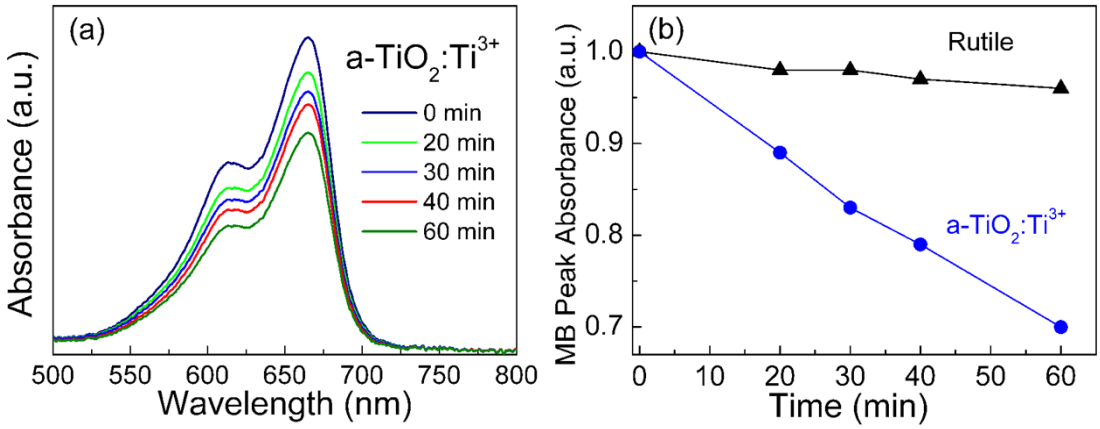

Figure S2. (a) Absorption spectra of photocatalytically degraded methylene blue (6×10^{-5} M) as a function of irradiation time in the presence of a-TiO_2:Ti^{3+} nanoparticles under Xe lamp (400 nm long pass filter) irradiation (b) Photodegradation kinetics of methylene blue using rutile nanoparticles (average size: ~ 35 nm) and a-TiO_2:Ti^{3+} nanoparticles .

In order to further understand the visible light response of a-TiO_2:Ti^{3+}, the photocatalysis property of a-TiO_2:Ti^{3+} was also investigated, as shown in Figure S2. The photodegradation of the methylene blue (MB) by rutile and a-TiO_2:Ti^{3+} nanoparticles were carried out under the irradiation of Xe lamp using 400 nm long pass filter for different time interval. As compared with rutile TiO_2, the a-TiO_2:Ti^{3+} nanoparticles exhibit unambiguous visible light photocatalysis property, as shown in Supplementary Fig. S2.

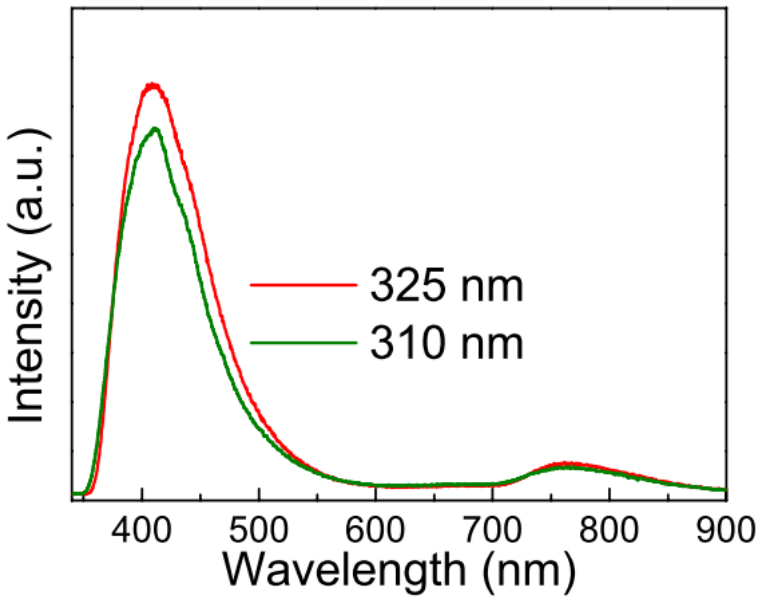

Figure S3. PL spectra of TiO_2: Ti^{3+} under different excitation wavelength

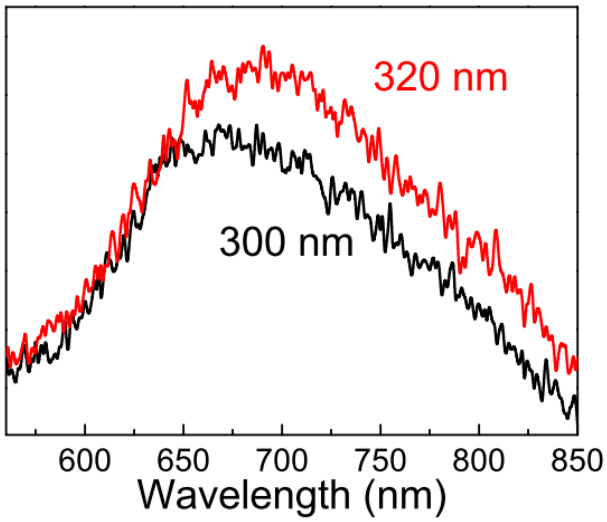

Figure S4. Defect emission spectra of pristine TiO_2 under different excitation wavelength (300 nm and 320 nm)

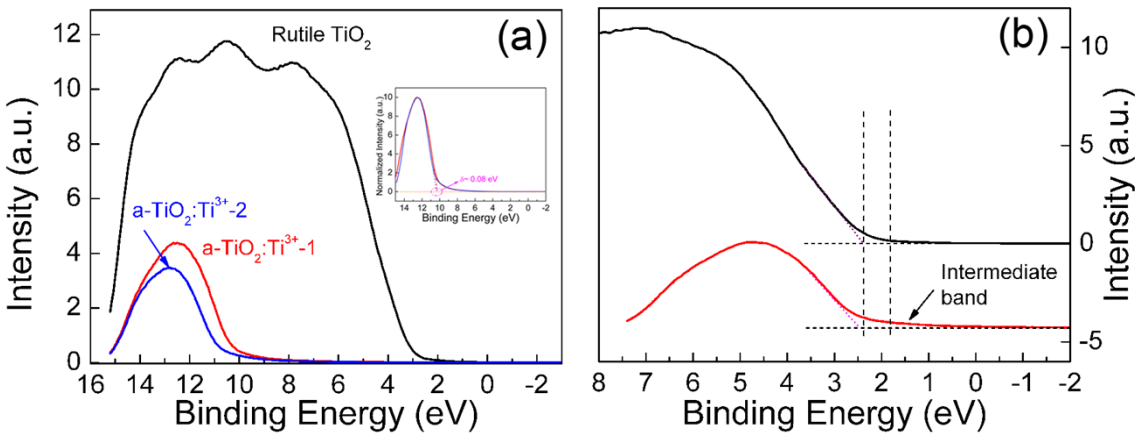

Figure S5. UPS results of rutile and a-TiO_2:Ti^{3+} (a) original data, inset, normalized UPS spectra of a-TiO_2:Ti^{3+}, the error is less than the energy resolution of UPS facility (~ 0.1 eV, ESCALAB 250, Thermo-VG Scientific), (b) Corrected UPS binding energy based on the XPS-VBS results.

In Figure S5, the a-TiO_2:Ti^{3+}-1 and a-TiO_2:Ti^{3+}-2 are the same sample, which is recorded for the first time and second times in UPS experiment. The divergence between a-TiO_2:Ti^{3+}-1 and a-TiO_2:Ti^{3+}-2 can be attributed to the influence of UV light-generated electrons, which may increase the Fermi level. The surface charging effect in UPS measurement can not be effectively inner-corrected. In XPS VBS measurement, the surface charging can be internally corrected by C 1s binding energy. As compared with the rutile, the long tail at low binding energy side (0~1.8 eV) in a-TiO_2:Ti^{3+} indicates the existence of intermediate band electronic states within the band gap.

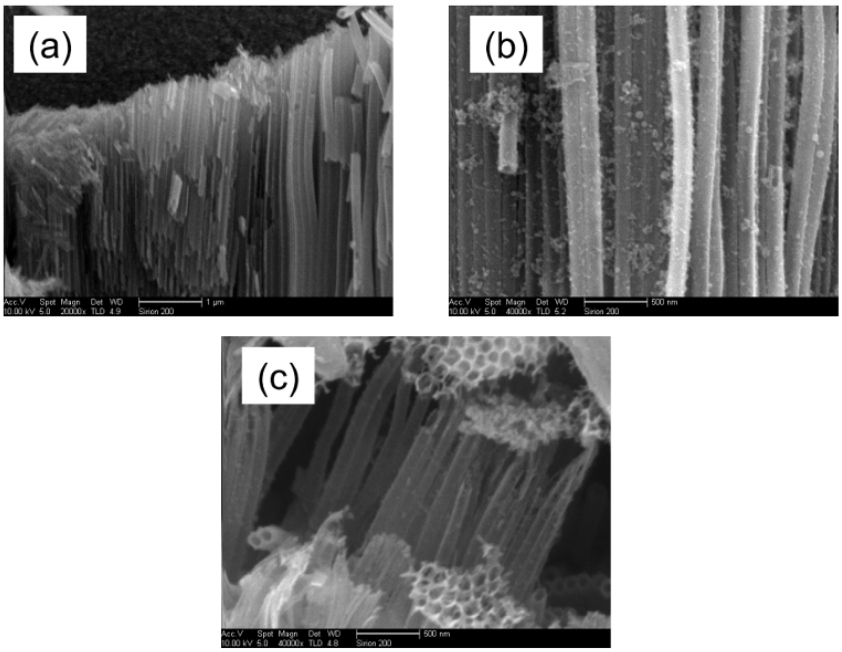

Figure S6. SEM images of TiO_2 NTs arrays before after grafted by TiO_2:Ti^{3+} nanoparticles. (a) TiO_2 NTs, TiO_2 NTs soaking in TiO_2:Ti^{3+} solutions for 2 hours under irradiation of 365 nm UV lamp (b) and in darkness (c).

The area coverage of a-TiO_2:Ti^{3+} is estimated from the FESEM image. The total amounts $N_{\text{a-TiO2:Ti3+ nanoparticles}}$ of a-TiO_2:Ti^{3+} nanoparticles can be counted. The average diameter of nanoparticles is 30 nm, the sectional area of one nanoparticle is 3.14x30x30= 2826 nm^2, and the total area of nanoparticles is 2826 $N_{\text{a-TiO2:Ti3+ nanoparticles}}$ nm^2. In the same SEM image with width W and length L, the area of packed nanotubes can be calculated $W{\cdot}L$ nm^2. Thus the area coverage of a-TiO_2:Ti^{3+} nanoparticles on TiO_2 nanotubes can be determined by the formula: $2826{\cdot}N_{\text{a-TiO2:Ti3+ nanoparticles}}/\ W{\cdot}L$.

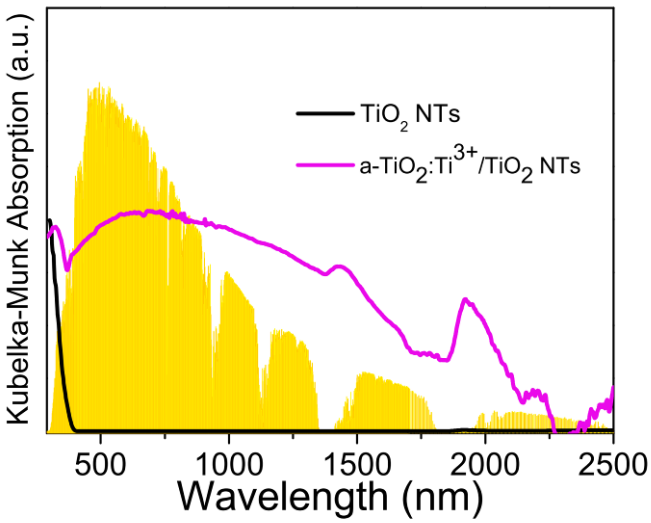

Figure S7. Absorption spectra of TiO_2 nanotubes (TiO_2 NTs) and a-TiO_2:Ti^{3+}-grafted TiO_2 NTs. The AM1.5G solar spectrum is drawn as the background.

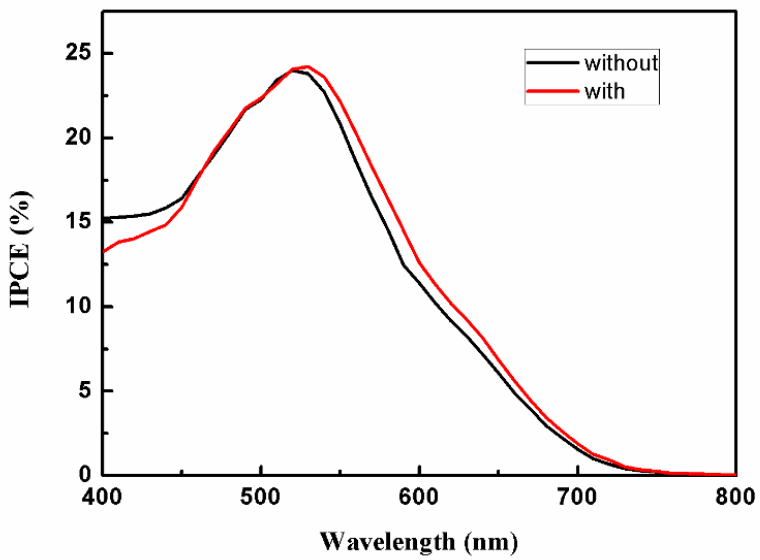

Figure S8. Typical IPCE curves of TiO_2 NTs DSSCs with and without decorating the TiO_2: Ti^{3+} nanoparticles. The soaking time is 30 min.

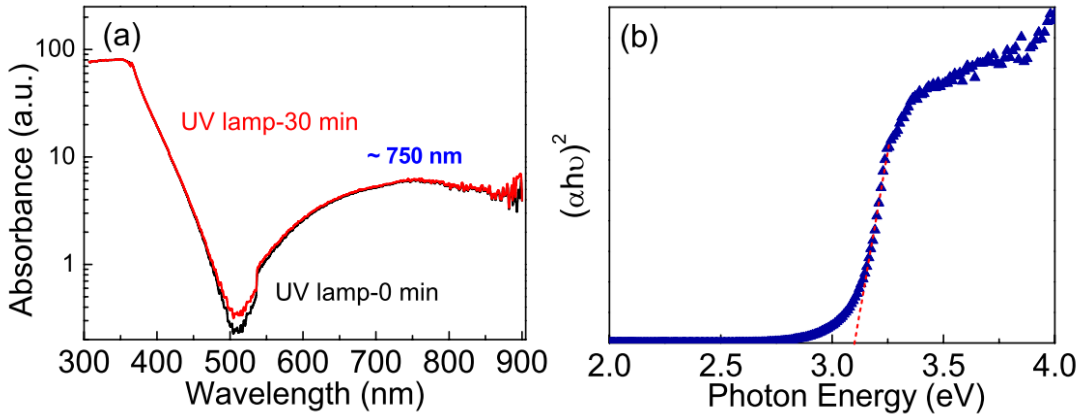

Figure S9. (a) Typical absorption spectrum of a-TiO_2:Ti^{3+} colloidal solution, red line: absorbance of a-TiO_2:Ti^{3+} colloidal solution after 8 W 365 nm UV lamp irradiation.; (b) Tauc plot $(\alpha h\nu)^2 \sim h\nu$ for the a-TiO_2:Ti^{3+} colloidal solution.

The band gap calculated based on the absorption spectra of colloidal solution is 3.06 eV, which is well consistent with the value determined by the reflectivity spectrum (3.04 eV).

Table S1. Fitted PL decay parameters for rutile TiO_2 and a-TiO_2: Ti^{3+} samples

PL decay profiles were fitted by two exponential function equation: $I(t) = t_0 + A_1 * \exp(-t/\tau_1) + A_2 * \exp(-t/\tau_2)$. τ_1 and τ_2 denote the decay time for the faster and the slower components, and A_1 and A_2 are the PL amplitudes.

Sample	t_0 (ns)	τ_1 (ns)	τ_2 (ns)	A_1	A_2	R-Square
Rutile TiO_2 (at 410 nm)	25	0.49	33	11205	146	0.993
TiO_2: Ti^{3+}(at 410 nm)	13	0.49	26	9715	68	0.998
TiO_2: Ti^{3+}(at 770 nm)	80	0.49	710	7700	1660	0.995

Table S2. XPS peaks fitted results of a-TiO_2: Ti^{3+} sample

Peaks	**Energy (eV)**	**FWHM (eV)**	**Area**
2p3/2(Ti^{4+})	458.9	1.176	31229
2p3/2(Ti^{3+})	457.4	1.627	4734
2p1/2(Ti^{4+})	464.7	1.588	10895
2p1/2(Ti^{3+})	463.2	2.351	2024

Proposed Formation Mechanism of Amorphous TiO_2 Grown by Pulsed Laser Ablation in Water

In the fabrication process, only rutile TiO_2 and H_2O were used as the precursor. The intermediate band state is related to the hydrogen impurity. According to the theoretical calculation [PRL 111, 065505 (2013)], the hydrogen acts as important role in forming the disordered TiO_2. And the lattice disorder in TiO_2 is attributed to originate from the hydrogenation that helps to break up Ti-O bonds of rutile nanocrystals by forming Ti-H and O-H bonds. The H_2 possibly comes from the water photolysis by rutile TiO_2 (band gap: ~ 410 nm) under the irradiation of 355 nm UV laser. And the H_2 react with rutile TiO_2 to form disorder lattice under high temperature and high pressure at the local sites caused by the high power pulsed laser.

References:

1 Pattier, B., Henderson, M., Poeppl, A., Kassiba, A. and Gibaud, A. Multi-approach Electron Paramagnetic Resonance Investigations of UV-Photoinduced Ti3+ in Titanium Oxide-Based Gels. *J. Phys. Chem. B* **114**, 4424-4431 (2010).

2 Cottineau, T., Brohan, L., Pregelj, M., Cevc, P., Richard-Plouet, M. and Arčon, D. Evidence of Interfacial Charge Transfer upon UV-Light Irradiation in Novel Titanium Oxide Gel. *Adv. Funct. Mater.* **18**, 2602-2610 (2008).

3 Su, J., Zou, X.-X., Zou, Y.-C., Li, G.-D., Wang, P.-P. and Chen, J.-S. Porous Titania with Heavily Self-Doped Ti^{3+} for Specific Sensing of CO at Room Temperature. *Inorg. Chem.* **52**, 5924-5930 (2013).

4 Zhang, X. B., Tian, H. M., Wang, X. Y., Xue, G. G., Tian, Z. P., Zhang, J. Y., Yuan, S. K., Yu, T. and Zou, Z. G. The role of oxygen vacancy-Ti3+ states on TiO2 nanotubes' surface in dye-sensitized solar cells. *Mater. Lett.* **100**, 51-53 (2013).

5 Cottineau, T., Rouet, A., Fernandez, V., Brohan, L. and Richard-Plouet, M. Intermediate band in the gap of photosensitive hybrid gel based on titanium oxide: role of coordinated ligands during photoreduction. *Journal of Materials Chemistry A* **2**, 11499-11508 (2014).